JCI insight

JAML promotes acute kidney injury mainly through a macrophage-dependent mechanism

Wei Huang, Bi-Ou Wang, Yunfeng Hou, Yi Fu, Sijia Cui, Jinghan Zhu, Xinyu Zhan, Rongkun Li, Wei Tang, Jichao Wu, Ziying Wang, Mei Wang, Xiaojie Wang, Yan Zhang, Min Liu, Yusheng Xie, Yu Sun, Fan Yi

JCI Insight. 2022. https://doi.org/10.1172/jci.insight.158571.

Research In-Press Preview **Nephrology**

Graphical abstract

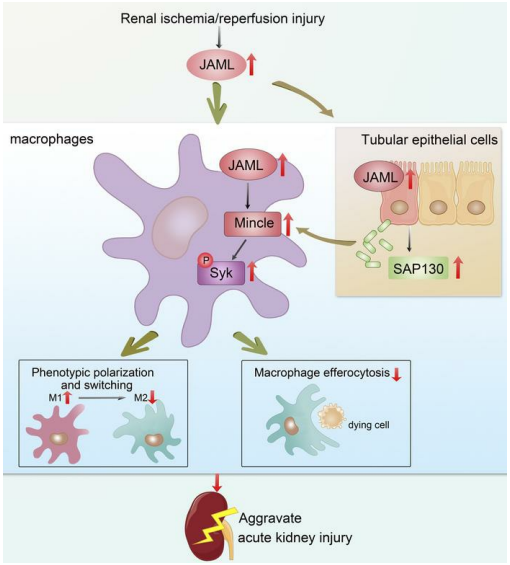

158571-INS-RG-RV-2

JAML promotes acute kidney injury mainly through a macrophage-dependent mechanism

Wei Huang[1], Bi-Ou Wang[1], Yun-Feng Hou[2], Yi Fu[1], Si-Jia Cui[1], Jing-Han Zhu[1], Xin-Yu Zhan[1], Rong-Kun Li[1], Wei Tang[3], Ji-Chao Wu[1], Zi-Ying Wang[1], Mei Wang[1], Xiao-Jie Wang[1], Yan Zhang[1], Min Liu[1], Yu-Sheng Xie[1], Yu Sun[1*] and Fan Yi[1,4*]

[1]The Key Laboratory of Infection and Immunity of Shandong Province, Department of Pharmacology, School of Basic Medical Sciences, Shandong University, Jinan, China.
[2]Intensive Care Unit, Shandong Provincial Qianfoshan Hospital, the First Affiliated Hospital of Shandong First Medical University, Jinan, China.
[3]Department of Pathogenic Biology, School of Basic Medical Sciences, Shandong University, Jinan, China.
[4]Key Laboratory of Cardiovascular Remodeling and Function Research, Chinese Ministry of Education and Chinese Ministry of Health, and The State and Shandong Province Joint Key Laboratory of Translational Cardiovascular Medicine, Qilu Hospital, Shandong University, Jinan, China.

Running titles: JAML and acute kidney injury

* Correspondence to: Fan Yi or Yu Sun
Department of Pharmacology
School of Basic Medical Sciences
Shandong University
44# Wenhua Xi Road, Jinan, Shandong 250012, China
Phone: 86-531-88382036
E-mail: fanyi@sdu.edu.cn or sy5409@sdu.edu.cn

Conflict of interest. The authors have declared that no conflict of interest exists.

Abstract

Although macrophages are undoubtedly attractive therapeutic targets for acute kidney injury (AKI) because of their critical roles in renal inflammation and repair, the underlying mechanisms of macrophage phenotype switching and efferocytosis in the regulation of inflammatory responses during AKI are still largely unclear. The present study was to elucidate the role of JAML (junctional adhesion molecule-like protein) in the pathogenesis of AKI. We found that JAML was significantly up-regulated in the kidney from two different murine AKI models including renal ischemia/reperfusion injury (IRI) and cisplatin-induced AKI. By generation of bone marrow chimeric mice, macrophage-specific and tubular-specific *Jaml* conditional knockout mice, we demonstrated JAML promotes AKI mainly via a macrophage-dependent mechanism and found that JAML-mediated macrophage phenotype polarization and efferocytosis is one of critical signal transduction pathways linking inflammatory responses to AKI. Mechanistically, the effects of JAML on the regulation of macrophages was at least in part, associated with a Mincle-dependent mechanism**.** Collectively, our studies for the first time explore new biological functions of JAML in macrophages and conclude that JAML is an important mediator and biomarker of AKI. Pharmacologic targeting of JAML mediated signaling pathways at multiple levels may provide a novel therapeutic strategy for patients with AKI.

Key words: Junctional adhesion molecule; Acute kidney injury; Mincle; Macrophage; Efferocytosis

Introduction

Acute kidney injury (AKI), often caused by renal ischemia/reperfusion injury (IRI), nephrotoxic agents and sepsis, is a global public health concern associated with high morbidity and mortality (1, 2). Currently, other than dialysis, no therapeutic interventions reliably improve survival, limit injury, or speed recovery after AKI (3). Numerous studies have demonstrated that the inflammatory response plays a vital role in the pathogenesis of various AKI (4-6) . Thus, better understanding of the cellular and molecular mechanisms underlying the inflammatory response has high potential for identifying effective therapies to prevent or ameliorate AKI. During AKI, a complex network of interactions among recruited immune cells, resident immune cells and renal parenchymal cells sets major innate immunity pathways in motion by activating pattern recognition receptors (PRR) and releasing various inflammatory mediators (7-10). Among inflammatory myeloid cells, macrophages are undoubtedly attractive therapeutic targets for AKI because of their critical roles in renal inflammation and repair (11-15). Macrophages are highly heterogeneous and their differentiation into morphologically and functionally distinct phenotypes M1/M2 depending on the microenvironment and the nature or the stage of disease (16). Inflammatory M1 macrophages are recruited to the kidney where they amplify inflammatory responses and promote parenchymal injury. In contrast, M2 macrophages show anti-inflammatory effects after AKI and facilitate renal repair (17). In the process of inflammation resolution, a process termed 'efferocytosis' for the clearance of apoptotic or dying cells by macrophages is also essential for maintaining tissue homeostasis (18, 19). Accordingly, defective efferocytosis exacerbates autoimmune diseases and sterile inflammation (20, 21). However, the underlying mechanisms of M1 and M2 macrophage phenotype switching and efferocytosis in the regulation of inflammatory responses during AKI are still largely unclear.

Therefore, identification of key factors controlling the phenotype and functions of macrophages may offer a new avenue for the development of therapeutic strategies for patients with AKI.

Recently, the role of junctional adhesion molecules (JAMs) of the immunoglobulin superfamily has attracted much attention because of their important functions on immune cell activation and inflammatory responses (22, 23). JAMs are expressed by leukocytes, platelets, epithelial and endothelial cells, and play critical roles in the regulation of cell polarity, epithelial barrier formation and leukocytes migration (22-25). Junctional adhesion molecule–like protein (JAML), as a novel identified member of the JAM family, is expressed on a variety of effector cells of both innate and adaptive immunity including monocytes, neutrophils and memory T cells as well as some parenchyma cells (26-29). Emerging evidence has revealed that JAML is vital to regulate leukocytes adhesion and transendothelial migration and is a costimulatory receptor for epithelial γδ T cell activation (26, 27, 30, 31), indicating the potential role of JAML in triggering the inflammation and tissue repair. However, the contribution of JAML to AKI and its regulation of macrophage dynamics and functions is still unknown. In this study, we explored the new biological functions of JAML in promoting AKI and JAML-mediated macrophage phenotype polarization and efferocytosis is one of critical signal transduction pathways linking inflammatory responses to AKI, suggesting that JAML may be an attractive therapeutic target and biomarker for AKI.

Results

JAML was upregulated in the kidney from patients with AKI and mice with renal IRI. By immunohistochemical (IHC) staining analysis (Figure 1A), we firstly observed the up-regulation of JAML in the kidney from patients with biopsy-proven acute tubular necrosis (ATN), which presents with AKI and is one of the most common causes of AKI. We also found that JAML was not only localized in the renal interstitium, but also expressed and induced in renal parenchymal cells after AKI (Figure 1A). By fluorescent multiplexed IHC consecutive staining on single slide, we further determined JAML expression in macrophages in the interstitum (Figure 1B). In mice with renal IRI, JAML expression was elevated in the kidney after 30 min of renal ischemia followed by different time points of reperfusion in mice by mRNA (Figure 1C), Western blot (Figure 1D) and IHC (Figure 1, E and F) analyses. In addition, the serum level of JAML was also enhanced compared to their controls (Figure 1G).

JAML deficiency protected against renal injury and alleviated inflammatory responses in mice with renal IRI. By generation of global *Jaml* knockout (*Jaml*$^{-/-}$) mice, which was confirmed by mRNA (Supplemental Figure 1A), Western blot (Supplemental Figure 1B), and IHC staining (Supplemental Figure 1C) analyses in the kidney, we found that JAML deficiency significantly reduced renal IRI in mice as evidenced by decreased levels of serum creatinine (Supplemental Figure 1D) and blood urea nitrogen (Supplemental Figure 1E). As shown in Supplemental Figure 1F, in parallel with improved morphological injuries and reduced dying cells, the level of kidney injury molecule 1 (KIM-1) that is an early biomarker of AKI and correlated with kidney tissue damage, was also significantly reduced in *Jaml* $^{-/-}$ mice compared with wide-type (WT) mice with renal IRI. Furthermore, JAML deficiency attenuated inflammatory responses by decreasing macrophage and neutrophil infiltration (Supplemental

Figure 2A), the levels of proinflammatory mediators (Supplemental Figure 2, B-E) in the kidney from mice with renal IRI.

JAML in bone marrow-derived immune cells primarily contributed to renal IRI. Considering that JAML was not only expressed in immune cells such as macrophages but also in renal parenchymal cells, we next determined the contribution of JAML in bone marrow (BM) - derived immune cells or renal parenchymal cells individually to the pathogenesis of renal IRI by BM transplantation studies. The chimeric mice were created, in which BM was replaced with donor BM cells from WT or from *Jaml*$^{-/-}$ mice. Six weeks after BM transplantation, chimeric mice were subjected to renal IRI (Figure 2A). Meanwhile, by using green fluorescent protein (GFP)-transgenic mice as donor, BM reconstitution in the recipient mice was confirmed by flow cytometry analysis of GFP expression. The proportion of GFP-positive (GFP^{+}) cells in the reconstructed BM was about 80% (Figure 2B). WT→ WT chimeras developed renal injury after IRI as assessed by elevated serum creatinine (Figure 2C), blood urea nitrogen (Figure 2D) and tubular damage (Figure 2E, Supplemental Figure 3), as well as displayed the increase of renal cell death (Figure 2F). Notably, in comparison to WT→ WT chimeras, *Jaml* $^{-/-}$→ WT chimeras which lacked myeloid JAML significantly ameliorated renal IRI. Similar results were also found in *Jaml* $^{-/-}$→*Jaml* $^{-/-}$ chimeras compared to WT→ *Jaml* $^{-/-}$ mice. However, neither WT→*Jaml* $^{-/-}$ nor *Jaml* $^{-/-}$→*Jaml* $^{-/-}$ mice (lacking renal parenchymal JAML in recipient mice) had obvious damage reduction compared to WT→ WT or *Jaml* $^{-/-}$→WT chimeras respectively, although a reducing tendency was observed. Thus, the presence of JAML in immune cells worsened renal damage and appears to be a major contributor to AKI.

Macrophage JAML was required in the pathogenesis of AKI. Considering that macrophages and neutrophils are predominant myeloid cell types that play a critical role in renal inflammation

and repair following AKI (5, 6), we examined JAML expression on macrophages and neutrophils isolated from the kidney of mice with renal IRI by flow cytometry analysis. For macrophages, two subtypes were further identified based on the F4/80 and CD11b fluorescence intensity (32-37). Infiltrating macrophages, which arrive to the kidney from the peripheral blood are CD11b^{high} F4/80^{low} (F4/80^{low}). Resident macrophages, which are largely embryonic derived, are CD11b^{low} F4/80^{high} (F4/80^{high}) (Figure 3A). Then, gating on F4/80^{low} and F4/80^{high} populations of macrophages from the kidney in mice with renal IRI and their controls, we found that JAML was more significantly up-regulated on F4/80^{low} macrophages from the injured kidney compared to F4/80^{high} populations as shown by mean fluorescence intensity (MFI, Figure 3A). However, no appreciable changes of JAML expression were observed on neutrophils (Supplemental Figure 4A).

Moreover, we generated macrophage-specific *Jaml* knockout (*LysM-cre*$^{+}$/*Jaml*$^{fl/fl}$) mice by intercrossing *Jaml-floxed* mice with *LysM (Lyz2)-Cre* mice (Figure 3B, Supplemental Figure 4B). BM-derived macrophages (BMDMs) isolated from *LysM-cre*$^{+}$/*Jaml*$^{fl/fl}$ mice had an almost complete absence of JAML expression (Figure 3C). Consistently, *LysM-cre*$^{+}$/*Jaml*$^{fl/fl}$ mice following renal IRI exhibited obvious improvement in renal function (Figure 3, D and E), tubular injury and cell death (Figure 3F) in the kidney as compared with *LysM-Cre*$^{+}$/*Jaml*$^{+/+}$ mice, further confirming the pathological significance of macrophage JAML in AKI.

Renal tubule-specific JAML deletion in mice only slightly ameliorated renal IRI. We also generated renal tubule-specific knockout mice (*Ksp-Cre*$^{+}$/*Jaml*$^{fl/fl}$, Figure 4A), which was confirmed by tail genotyping (Figure 4B), Western blot analysis of isolated tubules (Figure 4C) and IHC staining in the kidney (Figure 4D), to further examine the contribution of JAML in renal tubular cells to renal IRI. *Ksp-Cre*$^{+}$/*Jaml*$^{fl/fl}$ mice were phenotypically normal and had no

appreciable defect in renal morphology and function compared to *Ksp-Cre*$^{+}$*/Jaml*$^{+/+}$ littermates. However, *Ksp-Cre*$^{+}$*/Jaml*$^{fl/fl}$ mice following renal IRI exhibited a trend of improvements in renal function (Figure 4, E and F), tubular injury (Figure 4, G and H) and cell death (Supplemental Figure 5) in the kidney as compared with *Ksp-Cre*$^{+}$*/Jaml*$^{+/+}$ mice, but no significant difference.

JAML facilitated C-type lectin receptor Mincle signaling. By microarray analysis of global gene expression in the kidney from *Jaml* $^{-/-}$ mice with renal IRI, we found notable changes in some members of C-type lectin receptors (CLRs) which belong to a family of PRRs (Figure 5A). Among them, real time RT-PCR (Figure 5B) and Western blot (Figure 5C) analyses further verified that JAML deficiency markedly attenuated IR-induced macrophage-inducible C-type lectin (Mincle, also called *Clec4e*) expression in the kidney, but no significant effects on other CLRs such as *Clec4d, Clec1b, Clec2h, Clec7a, Clec9a* and *Clec12a* (Figure 5B). In consistent with previous studies showing that Mincle is selectively expressed and induced in macrophages (38) after AKI, we found that Mincle expression is obviously lower in macrophages isolated from the kidney of *Jaml*$^{-/-}$ mice compared to that from WT mice by flow cytometry analysis (Figure 5D). Consistently, by IHC staining analysis (Supplemental Figure 6A), Mincle expression was markedly decreased in the interstitium of injured kidney in *LysM-cre*$^{+}$*/Jaml*$^{fl/fl}$ mice relative to *LysM-Cre*$^{+}$*/Jaml*$^{+/+}$mice.

To elucidate the role of JAML in macrophages, we firstly treated BMDMs with LPS and confirmed the enhanced expression of JAML on macrophages in vitro (Supplemental Figure 6B). JAML deficiency on BMDMs isolated from *Jaml*$^{-/-}$ mice (Figure 5E) alleviated inflammatory responses under LPS treatment (Figure 5, F-I). In consistent with in vivo results, we observed a significant change of Mincle expression by mRNA (Supplemental Figure 6C) and Western blot analyses (Figure 5J) in BMDMs. Moreover, JAML deficiency inhibited the activation of spleen

tyrosine kinase (Syk), a well-recognized direct downstream effector of Mincle (Figure 5J), which was reversed by Mincle overexpression (Supplemental Figure 6, D and E).

JAML regulated macrophage phenotypic polarization and efferocytosis via a Mincle-dependent mechanism. Next, we polarized BMDMs isolated from WT or *Jaml*$^{-/-}$ mice into M1 or M2 macrophages, before switching them back into M2 or M1 macrophages, respectively. A panel of specific M2 or M1 marker genes was quantified by real-time RT-PCR. In the absence of JAML, M1 macrophages that had been switched to M2 showed significantly enhanced expressions of M2-associated genes *Arg1* and *Ccl8* (Figure 6A), while JAML-deficient M2 macrophages that had been switched to M1 showed lower expression of M1-related genes *Il6* and *iNos* (Figure 6B). All of these changes were counteracted by Mincle overexpression (Figure 6, A and B). Similar results were further verified by ELISA (Supplemental Figure 7A).

We also tried to assess the effect of JAML on macrophage polarization *in vivo*. As previous studies described (39, 40), we detected the polarization status of two subtypes of macrophages, F4/80^{low} (infiltrating) and F4/80^{high} (resident), in the mouse kidney by flow cytometry analysis. It was found a significantly higher proportion of M2 (CD206^{high}) or lower proportion of M1 (CD80^{high}) macrophages in *Jaml*$^{-/-}$ IRI mice than in control mice (Figure 6C, Supplemental Figure 7B). In addition, the MFI of CD80 or CD86, two markers of M1-like macrophages, was significantly decreased, while CD206 (M2 marker) was increased in *Jaml*$^{-/-}$ mice than that in WT littermates after renal IRI. Of note, JAML deficiency promotes phenotypic polarization toward M2, which was much more apparently in infiltrating macrophages than that in resident macrophages (Figure 6D, Supplemental Figure 7C).

In addition, we also found that JAML-Mincle signaling regulated macrophage efferocytosis. To evaluate the efferocytic capacity of peritoneal macrophages in vivo, we injected the peritoneum

with fluorescently labeled apoptotic neutrophils. After 45 min, the peritoneal cells were collected and analyzed by flow cytometry (Figure 7A). Uptake of the injected apoptotic neutrophils by $F4/80^+$ macrophages in *Jaml*$^{-/-}$ mice was higher than that in WT mice (Figure 7B). Moreover, in vitro, we induced apoptosis in PKH67-labeled Jurkat cells via exposure to UV radiation (Figure 7C) and then administrated the apoptotic cells to BMDMs for 2h and washed the cultures to remove any free apoptotic cells. Fluorescent microscopy was employed to assess efferocytosis. Our data showed that macrophages from *Jaml*$^{-/-}$ mice had significantly higher efferocytosis than those from WT mice, which was reversed by overexpression of Mincle (Figure 7D).

To further investigate that JAML modulated macrophage efferocytosis through Mincle during AKI, kidney sections were double-stained in situ with TUNEL reagents and CD68 antibody based on previous studies (41, 42). As expected, the injured kidney of *Jaml*$^{-/-}$ mice had a higher ratio of macrophage-associated TUNEL+ apoptosis cells to free apoptosis cells compared to WT mice, even though the number of macrophages was reduced (Supplemental Figure 7D). Moreover, after Mincle was significantly over-expressed in macrophages from *Jaml*$^{-/-}$ mice as determined by Western blot analysis (Supplemental Figure 7E), adoptive transfer of macrophages was performed in recipient mice with AKI where chemical deletion of macrophages was achieved by clodronate-liposome. We found that the macrophage efferocytosis was markedly enhanced in the injured kidney of *Jaml*$^{-/-}$ mice who received *Jaml* deficient macrophages compared with control mice. These effects were significantly inhibited by adoptive transfer with Mincle overexpressed Jaml deficient macrophages (Supplemental Figure 7F), suggesting that JAML attenuated macrophage efferocytosis through Mincle during AKI.

Gene silencing of JAML inhibited the release of endogenous Mincle ligands from proximal tubule epithelial cells. Since that JAML was up-regulated in renal tubules under ischemic condition and renal tubule deletion of JAML seemed to lead to a slight protective effect, we then detected the role of JAML in NRK-52E cells. We used three approaches to mimic the hypoxia conditions including oxygen-glucose deprivation (OGD) (Supplemental Figure 8A), chemical anoxia/recovery induced by incubating cells in glucose-free medium with antimycin A/2-deoxyglucose for ATP depletion (anoxia) and then in glucose-replete complete growth medium (recovery) (Supplemental Figure 8B) or $CoCl_2$ treatment (Supplemental Figure 8C). All of these manipulations significantly induced JAML expression. Interestingly, although gene silencing of *Jaml* (Supplemental Figure 8D) had no obvious effects on OGD-induced cell apoptosis (Supplemental Figure 8E) and the expression of spliceosome-associated protein 130 (SAP130) (Supplemental Figure 8F), a nuclear protein and one of endogenous Mincle ligands (43, 44), it could significantly inhibit the release of SAP130 (Supplemental Figure 8G). These results suggest that JAML expressed in tubule cells slightly affects the activation of Mincle in macrophages probably by influencing the release of some endogenous ligands and participates in AKI.

JAML deficiency also protected against AKI induced by cisplatin. To confirm the broad implications of JAML signaling in the kidney, we sought to investigate whether JAML also plays a detrimental role in mice with AKI induced by cisplatin. It was found that JAML expression was also markedly increased in the kidney from mice after cisplatin injection (Figure 8A). Compared with controls, JAML deficiency ameliorated renal dysfunction (Figure 8, B and C), tubular injury and cell death (Figure 8D). Consistently, the levels of Mincle were also increased in the kidneys of mice with cisplatin treatment. JAML deficiency significantly

decreased Mincle expression (Figure 8, E-G). Taken together, these results indicate that up-regulation of JAML may be a common response in the kidney after AKI.

Discussion

Macrophages are undoubtedly attractive therapeutic targets for AKI, with their heterogeneity and plasticity providing both opportunities and challenges. The differentiation of macrophages into morphologically and functionally distinct phenotypes M1/M2 and their clearance of dead cells (efferocytosis) have been increasingly linked to renal inflammation and repair in AKI. Therefore, achieving the full therapeutic potential of macrophages for subjects with AKI requires a better understanding of the regulation of macrophage dynamics and functions. In this study, we found that JAML was significantly up-regulated in the kidney from two separate murine AKI models including renal IRI and cisplatin-induced AKI. *Jaml* deficiency markedly ameliorated renal dysfunction, histologic lesions, and inflammatory responses in mice with AKI. Consistently, a significant increase in JAML was also observed in human kidney sections from subjects with acute tubular necrosis, indicating that JAML may be a potential marker for AKI. More importantly, we demonstrated that JAML promoted AKI mainly through a macrophage-dependent mechanism. By generation of BM chimeric mice and tubule-specific *Jaml* knockout mice, we found that JAML in BM derived immune cells made more significant contributions to renal IRI, whereas JAML in renal parenchymal cells only has a slight influence on renal injury. Considering that macrophages and neutrophils are predominant myeloid cell types that play a critical role in renal inflammation and repair following AKI (5, 6), we further characterized the expression of JAML on renal macrophages and neutrophils individually. It was found that JAML was more significantly up-regulated on infiltrating macrophages from the injured kidney

compared to resident macrophages. However, no appreciable changes were observed on infiltrating neutrophils. Moreover, by generating macrophage-specific *Jaml* knockout mice which currently have a relatively high gene depletion efficiency in mature macrophages, we provided direct evidence to further confirm that JAML in macrophages was the major contributor to AKI.

Functionally, except our recent findings showing that JAML mediates podocyte lipid metabolism in the kidney (29), we further found that JAML regulated macrophage phenotype polarization in this study. Phenotypically polarized macrophages have the potential to switch their phenotype as tissue inflammation progresses and enters the resolution phase. However, the mechanisms that govern phenotypic polarization of macrophages and phenotypic switch are not well understood, although studies have reported that colony-stimulating factor-1, chemokine (C-C motif) receptor 5, and Kruppel-like factor 4, Yes-associated protein (YAP) might be the key regulators of the phenotypic switch (45-48). Here, we found that JAML not only maintained M1 phenotype of macrophages, but also critically inhibited the phenotype switching from M1 to M2. Despite in vivo systems where it has been seldom observed that macrophage populations polarize to the extent observed in vitro, to make our in vitro data more solid, we still tried to evaluate macrophages polarization in vivo in a way that was generally acceptable as previous studies described (39, 40). Consistently, JAML deficiency promoted phenotypic polarization toward M2 after renal IRI, which was more apparently in infiltrating macrophages than that in resident macrophages. Combined with the expression of JAML in two subtypes of macrophages after AKI, it is suggested that JAML in infiltrating macrophages may play a more important role in AKI than that in resident macrophages. However, given that JAML in resident macrophages was also increased after AKI and has a certain regulatory effect on macrophage polarization, our

current study could not exclude the role of resident macrophages JAML in AKI. Importantly, we also found that JAML deficiency promoted macrophage efferocytosis, which is a process for the clearance of dying cells by professional and non-professional phagocytes and is closely linked to macrophage heterogeneity, tissue homeostasis, and M2 polarization. Efferocytosis is not only a major role of M2 macrophages, but also can reinforce signaling pathways that reprogram macrophages toward an anti-inflammatory phenotype in a feed-forward fashion (18, 19). Accordingly, defective efferocytosis underlies a growing list of chronic inflammatory diseases (20, 21). Therefore, further understanding the aspects of JAML-mediated efferocytosis will shed light on the key pathophysiological processes in AKI and provide novel therapeutic strategies for diseases driven by defective efferocytosis and impaired inflammation resolution.

Mechanistically, JAML deficiency affected macrophage phenotype switching, phenotype polarization, and efferocytosis, which was at least in part, associated with a C-type lectin receptor Mincle-dependent mechanism**.** Mincle (macrophage-inducible C-type lectin) encoded by Clec4e, is a member of the C-type lectin receptor family and is involved in the initiation of innate immune response. Moreover, as a novel sensor of cell death, Mincle can also recognize damage-associated molecular patterns (DAMPs) and enable immune sensing of damaged self, which induce inflammatory responses and decrease dead cell clearance, thereby aggravating a vicious cycle of necroinflammation (49-51). Recent studies have indicated that Mincle is also involved in sustained inflammation after renal IRI (38). In this study, we found that JAML deficiency significantly reduced LPS- or AKI induced Mincle expression and the activation of its direct downstream effector Syk in BMDMs. We further provided direct evidence showing that Mincle functions as a key regulator linking JAML to macrophage inflammation.

It should be noted that JAML expression was also induced in renal tubular cells under pathogenic conditions and tubular-specific JAML deletion can slightly ameliorated renal IRI. Therefore, we speculated that the fate of tubular cells may be regulated by JAML. Unexpectedly, gene silencing of *Jaml* had no effect on hypoxia-induced tubular cell apoptosis. However, we found that JAML deficiency could inhibit the release of SAP130, which is one of the most important and common endogenous Mincle ligands released from dying cells under hypoxia conditions (43, 44). In fact, Mincle can recognize a series of ligands including SAP130, cholesterol crystals, cholesterol sulfate and β-glucosylceramide have been identified (52, 53) and has the capability of sensing endogenous and exogenous targets (51, 54). In terms of endogenous Mincle ligands, previous studies have shown that Mincle expressed on infiltrating macrophages senses dying renal tubular cells expressing β-glucosylceramide and inhibits macrophages phagocytic activity to induce sustained inflammation in AKI (51). In this study, we reported that JAML expressed in tubule cells can slightly affect the activation of Mincle in macrophages probably by influencing the release of the endogenous ligands and thereby participating in the process of AKI.

Collectively, we explore the novel biological functions of JAML in promoting AKI by regulating macrophage polarization and efferocytosis via Mincle (Figure 9), and further strengthen the concept that targeting macrophage may represent a novel therapeutic strategy for patients with AKI. Meanwhile, whether targeting JAML or macrophage therapy is sufficient to prevent renal damage in patients with AKI remains to be further established.

Materials and Methods

Human renal biopsy samples. Renal biopsies had been performed as part of routine clinical diagnostic investigation and the samples were obtained from Department of Pathology, Shandong University School of Basic Medical Sciences. We collected the human renal biopsy samples from patients with biopsy-proven acute tubular necrosis as described in Supplemental Table 1. None of these patients started dialysis therapy at the time of kidney biopsy. Normal control samples were obtained from healthy kidney poles of individuals who underwent tumor nephrectomies or renal cystectomy without other kidney diseases.

Mouse studies. WT (C57BL/6J) male mice were purchased from Vital River Laboratory Animal Technology Co., Ltd. Different groups were allocated in a randomized manner and investigators were blinded to the allocation of different groups when doing surgeries. All mice (3-5 mice per cage) were housed under standard laboratory conditions in the specific-pathogen-free experimental animal center of Shandong University. Male mice (27 ± 3 g; age 8–10 weeks) were used in this study. The number of the mice used for the experiments are indicated in the corresponding figure legends. All of our experimental animals were kept under barrier conditions under constant veterinary supervision and did not display signs of distress or pathological changes that warranted veterinary intervention.

Generation of global *Jaml* knockout mice. *Jaml*$^{flox/+}$ (*Jaml*$^{fl/+}$) mice (C57BL/6J;129) were generated by standard homologous recombination in Shanghai Southern Model Biotechnology Development Co., Ltd. (Shanghai, China). In these mice, exon 4 of *Jaml* was flanked by *loxP* sequences. Global *Jaml* knockout mice (*Jaml*$^{-/-}$) were obtained as described in our previous studies (29). Floxed *Jaml* mice with C57BL/6J;129 background were backcrossed with C57BL/6J mice more than 12 generations to produce congenic strains. Then, *Jaml*$^{fl/+}$ mice were

crossed with EIIa-Cre transgenic mice (C57BL/6J, Jackson Laboratory, Stock No.003724), in which the adenovirus EIIa promoter directs the expression of Cre enzyme in early mouse embryos (two- to eight-cell stage) to achieve homologous recombination between *LoxP* sites, thereby triggering the deletion of exon 4 in all cells of the developing animal, including the germ cells that transmit the genetic alteration to progeny. The first generation of EIIa-Cre *Jaml*$^{fl/+}$ mice might be chimeric due to the mosaic activity of Cre recombinase. Therefore, chimeric offspring were backcrossed with C57BL/6J to generate *Jaml*$^{+/-}$ mice, which were then intercrossed for the production of *Jaml*$^{-/-}$ mice. Mouse genotyping was performed using genomic DNA isolated from mouse tails by PCR (primers shown in Supplemental Materials, Supplemental Table 2).

Generation of macrophage-specific *Jaml* knockout mice. To obtain myeloid cell specific deletion of *Jaml*, *Jaml* homozygous floxed (*Jaml*$^{fl/fl}$, C57BL/6J backgrounds) mice were crossed with mice expressing Cre recombinase under the control of lysozyme 2 promoter (*LysM-Cre*, Jackson Laboratory, Stock No: 004781). Although *LysM* is not a specific marker for macrophages, *Lyz2 (LysM)-Cre* mice currently have a relatively high efficient gene depletion in mature macrophages and granulocytes isolated from peritoneal cavity or derived from bone marrow (55).

Generation of tubular-specific *Jaml* knockout mice. *Jaml*$^{fl/fl}$ mice (C57BL/6J backgrounds) were hybridized with transgenic mice expressing Cre-recombinase under the cadherin 16 promoter (*Ksp-Cre*) (Jackson Laboratory, Stock No: 012237) to generated tubular cell specific *Jaml* knockout mice (*Ksp-Cre*$^{+}$/*Jaml*$^{fl/fl}$). *Jaml*$^{fl/fl}$ and *Ksp-Cre* mice were all used in a C57BL/6 background. Age-matched mice with two wide type alleles and Cre expression were used as controls (*Ksp-Cre*$^{+}$/*Jaml*$^{+/+}$). Mouse genotyping was performed using genomic DNA isolated

from mouse tails by PCR at two weeks of age (primers shown in Supplemental Materials,Supplemental Table 2).

Generation of murine bone marrow chimeras. Donor mice were sacrificed. Tibias and femurs were flushed with medium (RPMI 1640 with 2% FBS, 10 units/mL heparin, 1% penicillin and streptomycin) as described in our previous studies (56). The mixture was passed through sterile 40μm nylon Cell Strainer (Falcon) and collected in a 50 mL tube. Cells were centrifuged at 900 x g 10 min at 4°C. The supernatant was discarded and the cell pellet was washed twice with 50 mL serum-free wash buffer (RPMI 1640 with 20 mM Hepes, 1% penicillin and streptomycin). After centrifugation, cells were resuspended in serum-free RPMI and cell number was determined using a cell counter (TC20^{TM} automated cell counter, Bio-Rad). Moreover, 8 weeks old recipient mice were lethally irradiated (9 Gy, once) and injected with 5×10^6 bone marrow (BM) cells (volume 0.2 mL) via the tail vein 6h after irradiation. Mice were kept on antibiotic (1g/L sulfamethazine in drinking water) for 2 weeks after irradiation and then switched to water without antibiotics. Using green fluorescent protein (GFP)-transgenic mice as donor to confirm the efficient replacement. In this experiments we used mice matched for age and genetic background and transplanted with appropriate BM (e.g. wide-type into wide-type) as controls.

Ischemia-reperfusion model of acute kidney injury. An established mouse model of renal ischemia / reperfusion injury (IRI) was performed as described previously (56, 57). Briefly, after mice were anesthetized with an intraperitoneal injection of pentobarbital sodium (30 mg/kg body weight), a midline abdominal incision was made and bilateral renal pedicles were clipped for 40 minutes using microaneurysm clamps. At the end of the ischemic period, the vascular clamps were removed (reperfusion) and the kidneys were observed for 5 minutes to ensure reflow process. The incision was then closed and the animal was allowed to recover. During the

ischemic period, body temperature was maintained between 36~37.5℃ using a temperature-controlled heating system. After reperfusion at 24 h, 48h and 72h, blood samples and kidneys were collected for subsequent analysis.

Cisplatin-induced model of acute kidney injury. Acute kidney injury in mice was also induced by a single intraperitoneal injection of cisplatin at a dose of 30 mg/kg (Sigma, St. Louis, MO). At 3d, 5d and 10d after injection, mice were sacrificed and kidney samples were collected for various analyses (56, 57).

Cell Culture and treatments. Bone marrow derived macrophages (BMDMs) were isolated from tibias and femurs of mice in a procedure similar to that used for the extraction of BMDMs in the bone marrow transplantation experiment. Bone marrow cells were cultured in Dulbecco's modified Eagle's medium (DMEM) supplemented with 10% FBS and macrophage colony-stimulating factor (M-CSF, 20ng/mL) under 37℃, 5% CO_2 conditions. Rat proximal tubule epithelial cells (NRK-52E) were purchased from American Type Culture Collection (ATCC) and cultured in DMEM containing 5% FBS and penicillin/streptomycin. Jurkat cells were kindly provided by Stem Cell Bank (Chinese Academy of Sciences, Shanghai, China) and cultured in DMEM supplemented with 10% FBS and 100 U/mL penicillin plus 0.1 mg/mL streptomycin.

Fluorescent multiplexed immunohistochemistry (F-MIHC). The sections were stained by using four-color F-MIHC Kit (Absin, Shanghai, China). As previously described (58), the slides were baked at 65 ℃ for 1 hour and deparaffinized in xylene and rehydrated in gradient concentration of ethanol. Antigen retrieval was performed in citrate buffer (pH 6.0) using microwave heating. The slides were then incubated with primary antibodies, followed by a secondary horseradish peroxidase-conjugated polymer that induces the covalent binding of different fluorophores via tyramide signal amplification (TSA). This reaction was followed by

additional antigen retrieval using citrate buffer in microwave to remove the primary and secondary antibodies. Each section was stained in two sequential rounds, then counterstained with DAPI and mounted with Anti-Fade Fluorescence Mounting Medium (Abcam). The expression of proteins of interest was evaluated as follows: JAML, Absin 520 TSA Plus; CD68, Absin 570 TSA Plus. Antibodies used in this study were summarized in Supplemental Table 3. The images were obtained by a LSM880 laser scanning confocal microscope (ZEISS, Germany) system.

Measurement of JAML level in mouse serum. As previously described (29), by using mouse JAML enzyme-linked immunosorbent assay (ELISA) Kit (Omnimabs, California, USA), the level of JAML in serum collected from mice were measured by Omnimabs (Shanghai, China) according to the manufacturer's instructions.

Assessment of renal function, histological analysis, immunofluorescence staining, real-time qRT-PCR, Western blot. These procedures were performed using standard techniques as described in Supplementary Materials.

Tissue dissociation and flow cytometry analysis. Mice were sacrificed and both kidneys were collected. Fresh kidneys were minced to small pieces and then placed in cold PBS with 1mg/mL collagenase IV and 2 U/mL DNase I after taking from control mice or mice with IRI. Shaking the tissues gently in a table concentrator with a constant temperature of 37℃ for 30 min. The cell suspension was centrifuged at 400g for 5 min after passing through 100μm strainer. Cell pellets were resuspended and washed with PBS and then monocyte were isolated by using density gradient centrifugation with Percoll (Solarbio P8370). Neutrophils were isolated with the EasySep Mouse Neutrophil Enrichment Kit according to manufacturer's instructions. The anti-CD16/CD32 antibody was used to block FcγRIII/II to minimize nonspecific antibody binding.

Cells were then stained by fluorescently conjugated antibodies (10^6 cells/1μg) that summarized in Supplemental Materials, Supplemental Table 3. Two subtypes of macrophages from the injured mouse kidney were analyzed based on the F4/80 and CD11b fluorescence intensity. Infiltrating macrophages are $CD45^+$ $CD11b^{high}$ $F4/80^{low}$. Resident macrophagesare $CD45^+$ $CD11b^{low}$ $F4/80^{high}$. Cell apoptosis was determined by propidiumiodide-annexinV staining as described (59). Flow cytometry was performed by CytoFLEX instrument (Beckman Coulter Biotechnology).

Isolation of renal tubules. Renal tubules was isolated by using a modified method for glomeruli isolation as described in our previous studies (60). In this protocol, the final pellet was resuspended and glomeruli containing Dynabeads were gathered by a magnetic particle concentrator after washing. The residual containing renal tubules were also collected. The extracted glomeruli and tubules were put aside respectively for protein analysis.

TUNEL assay. Cell death in the kidney after IRI was detected by TUNEL assay according to the manufacturer's protocol (Roche Diagnostics, Germany).

Microarray analysis. The microarray experiments were performed by Sinotech Genomics Corporation (Shanghai, China). Microarray data sets have been deposited to Gene Expression Omnibus under accession code (GSE192532).

Macrophages phenotype switching. BMDMs were used for phenotype switching after they were isolated from WT and *Jaml*$^{-/-}$ mice and cultured for 7 days. Isolated BMDMs were starved for 4h (M0) in medium without serum, and then polarized to M2 with IL-4 40 ng/mL or M1 with LPS 100 ng/mL. 8h later, M2 macrophages were then switched to M1 with LPS 100 ng/mL, and M1 macrophages were treated with M2 stimuli IL-4 40 ng/mL for another 8h. Cells were harvested for the extraction of mRNA and culture medium was collected for ELISA analysis

12h after the replacement of non-stimuli culture medium. The expression level of M1 or M2 markers were detected by qRT-PCR and ELISA analyses.

Macrophages efferocytosis assay in vivo. Neutrophils were collected by peritoneal lavage from donor mice 6 h after they had been injected with zymosan A. Neutrophils were isolated and then irradiated under ultraviolet (UV) lamp to induce apoptosis. Apoptotic neutrophils labeled with PKH26 red flourescent dye were injected into WT or *Jaml*$^{-/-}$ mice by intraperitoneal injection. 45 min later, the mice were sacrificed and the peritoneum was lavaged. Efferocytosis was analyzed by flow cytometry and quantified as the percentage of CD45^{+} CD11b^{+} F4/80^{+} macrophages that had taken up one or more PKH-labeled apoptotic cells.

In vitro macrophages efferocytosis assay. Jurkat cells were irradiated under a 254 nm UV lamp for 15 minutes to induce apoptosis, followed by incubation under normal cell culture conditions for 2-3h. This method routinely yields more than 85% apoptotic cells (ACs) as previously described (42). The ACs were resuspended at a concentration of 2 X 10^7 cells/mL, and incubated for 2 min with PKH26 red flourescent dye (PKH26 red flourescent cell linker, Sigma-Aldrich) (2μM/10^7 cells). Isolated BMDMs were plated in dishes and PKH26-labeled ACs were incubated with the macrophages for 45 min at a1: 5 macrophage: AC ratio. After 45 min, macrophages were washed three times with PBS to remove unbound ACs, and then the macrophages were fixed with 4% formaldehyde for 20 min. Images were taken by fluorescence microscopy and the percentage of BMDMs labeled with PKH26-tagged apoptotic Jurkat cells were quantified.

siRNA-mediated gene silencing and adenovirus-mediated gene expression. These procedures were provided in Supplementary Materials.

Statistics. Different groups of mice were allocated in a randomized manner and investigators were blinded to the allocation of different groups when doing surgeries and doing outcome evaluations. Exclusion criteria prior to the start of any of the in vivo studies were death, injury requiring euthanasia, or weight loss > 15%. Data are expressed as mean ± SEM. Statistical analyses were performed using GraphPad Prism 8.0. Normality assumption of the data distribution was assessed using Kolmogorov-Smirnov test. Comparisons between two groups were performed using two-tailed Student's unpaired t-test for normally distributed data and Mann-Whitney rank sum test for non-normally distributed data. Differences between multiple groups with one variable were determined using one-way ANOVA followed by post-hoc Tukey's test. To compare multiple groups with more than one variable, two-way ANOVA followed by post-hoc Tukey's test was used. For data with a non-Gaussian distribution, we performed a nonparametric statistical analysis using the Kruskal-Wallis test followed by the Dunn's post-hot test for multiple comparisons. Spearman's test was implemented for statistical analyses of the correlation between two variables. Statistical significance was defined as $*P < 0.05$, $**P < 0.01$, $***P < 0.001$.

Study approval. All human renal biopsy samples studies were conducted in accordance with the principles of the Declaration of Helsinki and were approved by the Research Ethics Committee of Shandong University after informed consent was obtained from the subjects. All experimental protocols for animal studies were approved by the Institutional Animal Care and Use Committee of School of Basic Medical Sciences, Shandong University (Document No. KYLL-2017(KS)-395) and conducted in accordance with the National Institutes of Health (NIH) Guide for the Care and Use of Laboratory Animals.

Data availability statement. Microarray data have been deposited in Gene Expression Omnibus (GSE192532). All other study data are included in the article and/or the Supplementary Materials. Additional data related to this paper may be requested from the authors.

Author contributions

Y.S. and F.Y. designed research; W.H., B.-O.W., Y.F., S.-J.C., J.-H.Z., X.-Y.Z., R.-K.L., J.-C.W., Z.-Y.W., M.W., X.-J.W. and M.L. performed research; W.H., Y.-F.H., X.-J.W., M.L., W.T., Y.Z., Y.-S.X., Y.S. and F.Y. analyzed data; Y.S. and F.Y. wrote the paper.

Acknowledgements

This study was supported by the National Science Fund for Distinguished Young Scholars to Y.F. (81525005); the National Key R&D Program of China (2020YFC2005000); the National Natural Science Foundation of China (82070753, 81770676, 91949202, 82090024, 82170734, 81873614, 81970580); Shandong Provincial Natural Science Foundation, China (ZR2019ZD40, ZR2019MH041).

Conflict of interest. The authors have declared that no conflict of interest exists.

References

1. Ronco C, et al. Acute kidney injury. *Lancet.* 2019;394(10212):1949-64.
2. Yang L, et al. Acute kidney injury in China: a cross-sectional survey. *Lancet.* 2015;386(10002):1465-71.
3. Levey AS, James MT. Acute Kidney Injury. *Ann Intern Med.* 2017;167(9):ITC66-ITC80.
4. Rabb H, et al. Inflammation in AKI: Current Understanding, Key Questions, and Knowledge Gaps. *J Am Soc Nephrol.* 2016;27(2):371-9.
5. Jang HR, Rabb H. Immune cells in experimental acute kidney injury. *Nat Rev Nephrol.* 2015;11(2):88-101.
6. Andrade-Oliveira V, et al . Inflammation in Renal Diseases: New and Old Players. *Front Pharmacol.* 2019;10:1192.
7. Tang PC, et al. The Emerging Role of Innate Immunity in Chronic Kidney Diseases. *Int J Mol Sci.* 2020;21(11).
8. Komada T, Muruve DA. The role of inflammasomes in kidney disease. *Nat Rev Nephrol.* 2019;15(8):501-20.
9. Wang YH, Zhang YG. Kidney and innate immunity. *Immunol Lett.* 2017;183:73-8.
10. Kurts C, et al . The immune system and kidney disease: basic concepts and clinical implications. *Nat Rev Immunol.* 2013;13(10):738-53.
11. Huen SC, Cantley LG. Macrophages in Renal Injury and Repair. *Annu Rev Physiol.* 2017;79:449-69.
12. Kumar S. Cellular and molecular pathways of renal repair after acute kidney injury. *Kidney Int.* 2018;93(1):27-40.
13. Han HI, et al. The role of macrophages during acute kidney injury: destruction and repair. *Pediatr Nephrol.* 2019;34(4):561-9.
14. Tang PM, et al. Macrophages: versatile players in renal inflammation and fibrosis. *Nat Rev Nephrol.* 2019;15(3):144-58.

15. Chen T, et al. M2 macrophages in kidney disease: biology, therapies, and perspectives. *Kidney Int.* 2019;95(4):760-73.

16. Cao Q, et al. Macrophage heterogeneity, phenotypes, and roles in renal fibrosis. *Kidney Int Suppl (2011).* 2014;4(1):16-9.

17. Watanabe S, et al. The role of macrophages in the resolution of inflammation. *J Clin Invest.* 2019;129(7):2619-28.

18. Morioka S, et al. Living on the Edge: Efferocytosis at the Interface of Homeostasis and Pathology. *Immunity.* 2019;50(5):1149-62.

19. Boada-Romero E, et al. The clearance of dead cells by efferocytosis. *Nat Rev Mol Cell Biol.* 2020;21(7):398-414.

20. Doran AC, et al. Efferocytosis in health and disease. *Nat Rev Immunol.* 2020;20(4):254-67.

21. Kourtzelis I, et al. DEL-1 promotes macrophage efferocytosis and clearance of inflammation. *Nat Immunol.* 2019;20(1):40-9.

22. Luissint AC, et al. JAM-related proteins in mucosal homeostasis and inflammation. *Semin Immunopathol.* 2014;36(2):211-26.

23. Reglero-Real N, et al. Endothelial Cell Junctional Adhesion Molecules: Role and Regulation of Expression in Inflammation. *Arterioscler Thromb Vasc Biol.* 2016;36(10):2048-57.

24. Ebnet K. Junctional Adhesion Molecules (JAMs): Cell Adhesion Receptors With Pleiotropic Functions in Cell Physiology and Development. *Physiol Rev.* 2017;97(4):1529-54.

25. Lauko A, et al. Junctional Adhesion Molecules in Cancer: A Paradigm for the Diverse Functions of Cell-Cell Interactions in Tumor Progression. *Cancer Res.* 2020;80(22):4878-85.

26. Witherden DA, et al. The junctional adhesion molecule JAML is a costimulatory receptor for epithelial gammadelta T cell activation. *Science.* 2010;329(5996):1205-10.

27. Luissint AC, et al. JAM-L-mediated leukocyte adhesion to endothelial cells is regulated in cis by alpha4beta1 integrin activation. *J Cell Biol.* 2008;183(6):1159-73.

28. Moog-Lutz C, et al. JAML, a novel protein with characteristics of a junctional adhesion molecule, is induced during differentiation of myeloid leukemia cells. *Blood.* 2003;102(9):3371-8.

29. Fu Y, et al. Elevation of JAML promotes diabetic kidney disease by modulating podocyte lipid metabolism. *Cell Metab.* 2020;32(6):1052-62 e8.

30. Guo YL, et al. Role of junctional adhesion molecule-like protein in mediating monocyte transendothelial migration. *Arterioscler Thromb Vasc Biol.* 2009;29(1):75-83.

31. McGraw JM, et al. JAML promotes CD8 and gammadelta T cell antitumor immunity and is a novel target for cancer immunotherapy. *J Exp Med.* 2021;218(10).

32. Yang Q, et al. Bone marrow-derived Ly6C(-) macrophages promote ischemia-induced chronic kidney disease. *Cell Death Dis.* 2019;10(4):291.

33. Lee S, et al. Distinct macrophage phenotypes contribute to kidney injury and repair. *J Am Soc Nephrol.* 2011;22(2):317-26.

34. Liu F, et al. Distinct fate, dynamics and niches of renal macrophages of bone marrow or embryonic origins. *Nat Commun.* 2020;11(1):2280.

35. Li L, et al. The chemokine receptors CCR2 and CX3CR1 mediate monocyte/macrophage trafficking in kidney ischemia-reperfusion injury. *Kidney Int.* 2008;74(12):1526-37.

36. Schulz C, et al. A lineage of myeloid cells independent of Myb and hematopoietic stem cells. *Science.* 2012;336(6077):86-90.

37. Lever JM, et al. Parabiosis reveals leukocyte dynamics in the kidney. *Lab Invest.* 2018;98(3):391-402.

38. Lv LL, et al. The pattern recognition receptor, Mincle, is essential for maintaining the M1 macrophage phenotype in acute renal inflammation. *Kidney Int.* 2017;91(3):587-602.

39. Miguel V, et al. Renal tubule Cpt1a overexpression protects from kidney fibrosis by restoring mitochondrial homeostasis. *J Clin Invest.* 2021;131(5).

40. Cao M, et al. Ginseng-derived nanoparticles alter macrophage polarization to inhibit melanoma growth. *J Immunother Cancer.* 2019;7(1):326.

41. Cai W, et al. STAT6/Arg1 promotes microglia/macrophage efferocytosis and inflammation resolution in stroke mice. *JCI Insight.* 2019;4(20).

42. Yurdagul A, Jr., et al. Macrophage Metabolism of Apoptotic Cell-Derived Arginine Promotes Continual Efferocytosis and Resolution of Injury. *Cell Metab.* 2020;31(3):518-33 e10.

43. Seifert L, et al. The necrosome promotes pancreatic oncogenesis via CXCL1 and Mincle-induced immune suppression. *Nature.* 2016;532(7598):245-9.

44. Lv LL, et al. SAP130 released by damaged tubule drives necroinflammation via miRNA-219c/Mincle signaling in acute kidney injury. *Cell Death Dis.* 2021;12(10):866.

45. Zhang MZ, et al. CSF-1 signaling mediates recovery from acute kidney injury. *J Clin Invest.* 2012;122(12):4519-32.

46. Liao X, et al. Kruppel-like factor 4 regulates macrophage polarization. *J Clin Invest.* 2011;121(7):2736-49.

47. Zhou X, et al. YAP Aggravates Inflammatory Bowel Disease by Regulating M1/M2 Macrophage Polarization and Gut Microbial Homeostasis. *Cell Rep.* 2019;27(4):1176-89 e5.

48. Alvarez JI, et al. JAML mediates monocyte and CD8 T cell migration across the brain endothelium. *Ann Clin Transl Neurol.* 2015;2(11):1032-7.

49. Richardson MB, Williams SJ. MCL and Mincle: C-Type Lectin Receptors That Sense Damaged Self and Pathogen-Associated Molecular Patterns. *Front Immunol.* 2014;5:288.

50. Yamasaki S, et al. Mincle is an ITAM-coupled activating receptor that senses damaged cells. *Nat Immunol.* 2008;9(10):1179-88.

51. Tanaka M, et al. C-type lectin Mincle mediates cell death-triggered inflammation in acute kidney injury. *J Exp Med.* 2020;217(11).

52. Kiyotake R, et al. Binds to Cholesterol Crystals and Triggers Innate Immune Responses. *J Biol Chem.* 2015;290(42):25322-32.

53. Kostarnoy AV, et al. Receptor Mincle promotes skin allergies and is capable of recognizing cholesterol sulfate. *Proc Natl Acad Sci U S A.* 2017;114(13):E2758-E65.

54. Behler-Janbeck F, et al. C-type Lectin Mincle Recognizes Glucosyl-diacylglycerol of Streptococcus pneumoniae and Plays a Protective Role in Pneumococcal Pneumonia. *PLoS Pathog.* 2016;12(12):e1006038.

55. Shi J, et al. Cre Driver Mice Targeting Macrophages. *Methods Mol Biol.* 2018;1784:263-75.

56. Li Q, et al. NLRC5 deficiency protects against acute kidney injury in mice by mediating carcinoembryonic antigen-related cell adhesion molecule 1 signaling. *Kidney Int.* 2018;94(3):551-66.

57. Fang W, et al. Gpr97 Exacerbates AKI by Mediating Sema3A Signaling. *J Am Soc Nephrol.* 2018;29(5):1475-89.

58. Seo YD, et al. Mobilization of CD8(+) T Cells via CXCR4 Blockade Facilitates PD-1 Checkpoint Therapy in Human Pancreatic Cancer. *Clin Cancer Res.* 2019;25(13):3934-45.

59. Liu M, et al. Sirt6 deficiency exacerbates podocyte injury and proteinuria through targeting Notch signaling. *Nat Commun.* 2017;8(1):413.

60. Fu Y, et al. Therapeutic Potential of Progranulin in Hyperhomocysteinemia-Induced Cardiorenal Dysfunction. *Hypertension.* 2017;69(2):259-66.

Figures

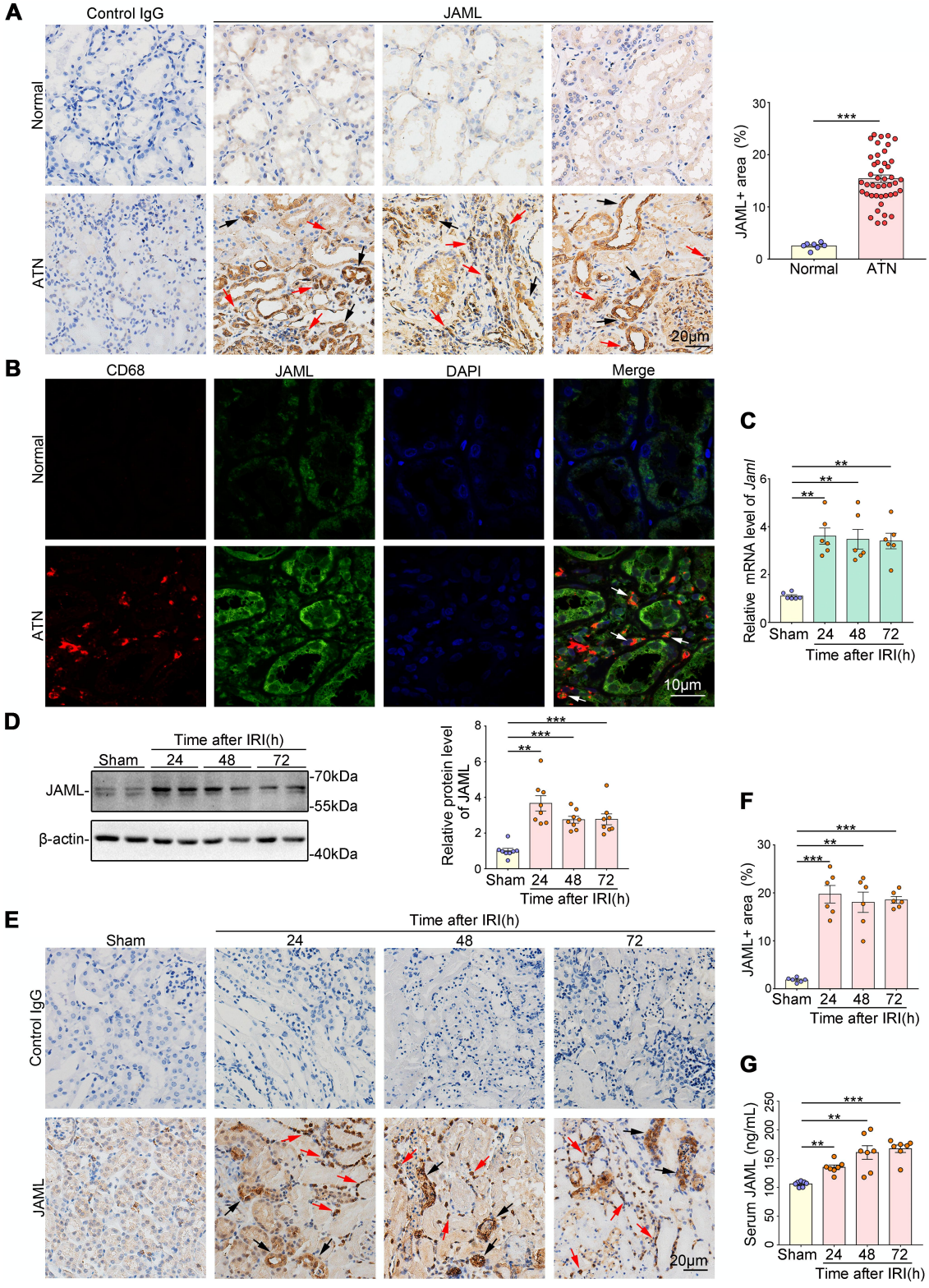
A
Control IgG
JAML
Normal
ATN
20μm
JAML+ area (%)
Normal
ATN
B
CD68
JAML
DAPI
Merge
10μm
C
Relative mRNA level of Jaml
Sham
24
48
72
Time after IRI(h)
D
Time after IRI(h)
JAML-
β-actin-
70kDa
55kDa
40kDa
Relative protein level of JAML
E
Time after IRI(h)
Control IgG
JAML
20μm
F
JAML+ area (%)
G
Serum JAML (ng/mL)

Figure 1. JAML was upregulated in the kidney from patients with AKI and mice with renal IRI. (A) Representative IHC images and quantification of JAML in the kidney from human normal kidney poles (n = 7), patients with biopsy-proven acute tubular necrosis (ATN) (n = 44). Red arrows indicate representative positive cells in renal interstitium; Black arrows indicate renal parenchymal cells. The kidney from human stained with normal IgG in place of the corresponding primary antibodies as a negative control. Scale bar: 20μm. **(B)** Representative fluorescent multiplexed IHC images of JAML (green) and CD68 (red) in the kidney from human normal kidney poles and patients with ATN (n = 6). Arrows indicate the expression of JAML in macrophages in renal interstitium. Scale bar: 10μm**. (C)** Relative mRNA level of *Jaml* in the kidney from mice with renal IRI (n = 6). **(D)** Representative Western blot and quantifications of JAML expression in the kidney from mice with renal IRI *(*n = 8). **(E)** Representative IHC images and quantification of JAML in the kidney from mice with renal IRI (n = 6). Red and black arrows indicate the same as in panel A. Scale bar: 20μm. **(F)** Serum level of JAML in mice with renal IRI (n = 7). Data are mean ± SEM. **P*<0.05, ***P*<0.01, ***P<0.001. Two-tailed Student's unpaired t test (A), One-way ANOVA test (C-F).

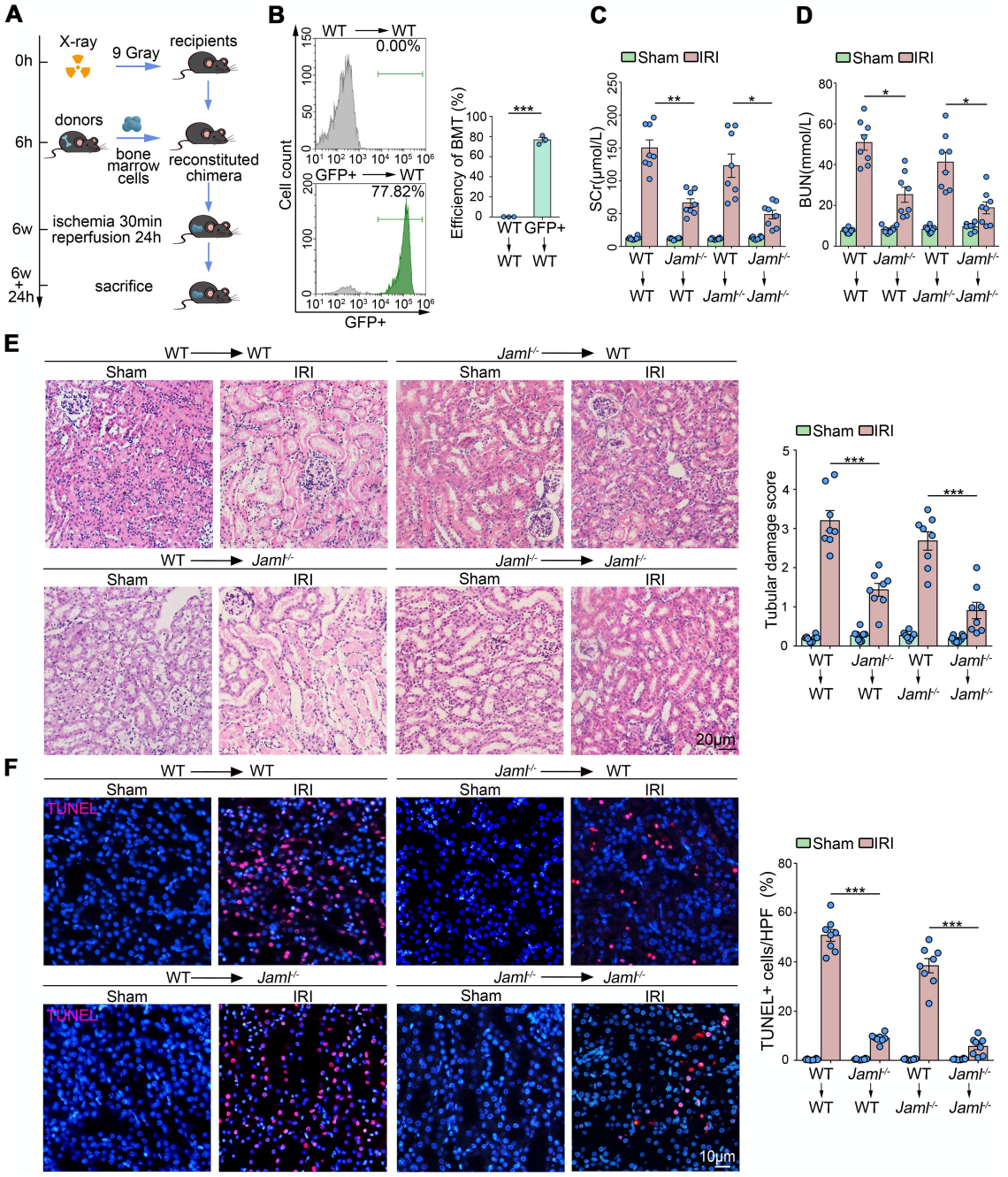

Figure 2. JAML in bone marrow-derived immune cells primarily contributed to renal IRI. (A) A schematic diagram showing the procedure of bone marrow transplantation for experimental mice. **(B)** Representative green fluorescent protein (GFP) expression profile of recipient bone marrow (BM) cells 6 weeks after BM transplantation by flow cytometry analysis. The proportion of GFP - positive (GFP^+) cells in the reconstructed BM was about 80% (n = 3). **(C)** Serum creatinine (SCr) concentration in different groups of mice after renal IRI (n = 8). **(D)** Blood urea nitrogen (BUN) levels of different groups of mice after renal IRI (n = 8). **(E)** Representative images of H&E staining showing the morphology of kidney and quantitative assessment of tubular damage in the kidney from different groups of mice (n = 8). Scale bar: 20μm. **(F)** In situ TUNEL assays and quantification were performed to assess renal cell death in the kidney from different groups of mice (n = 8). Scale bar: 10μm. Data are mean ± SEM. *P<0.05, **P<0.01, ***P<0.001. Two-tailed Student's unpaired t test (B), Two-way ANOVA test (C-F).

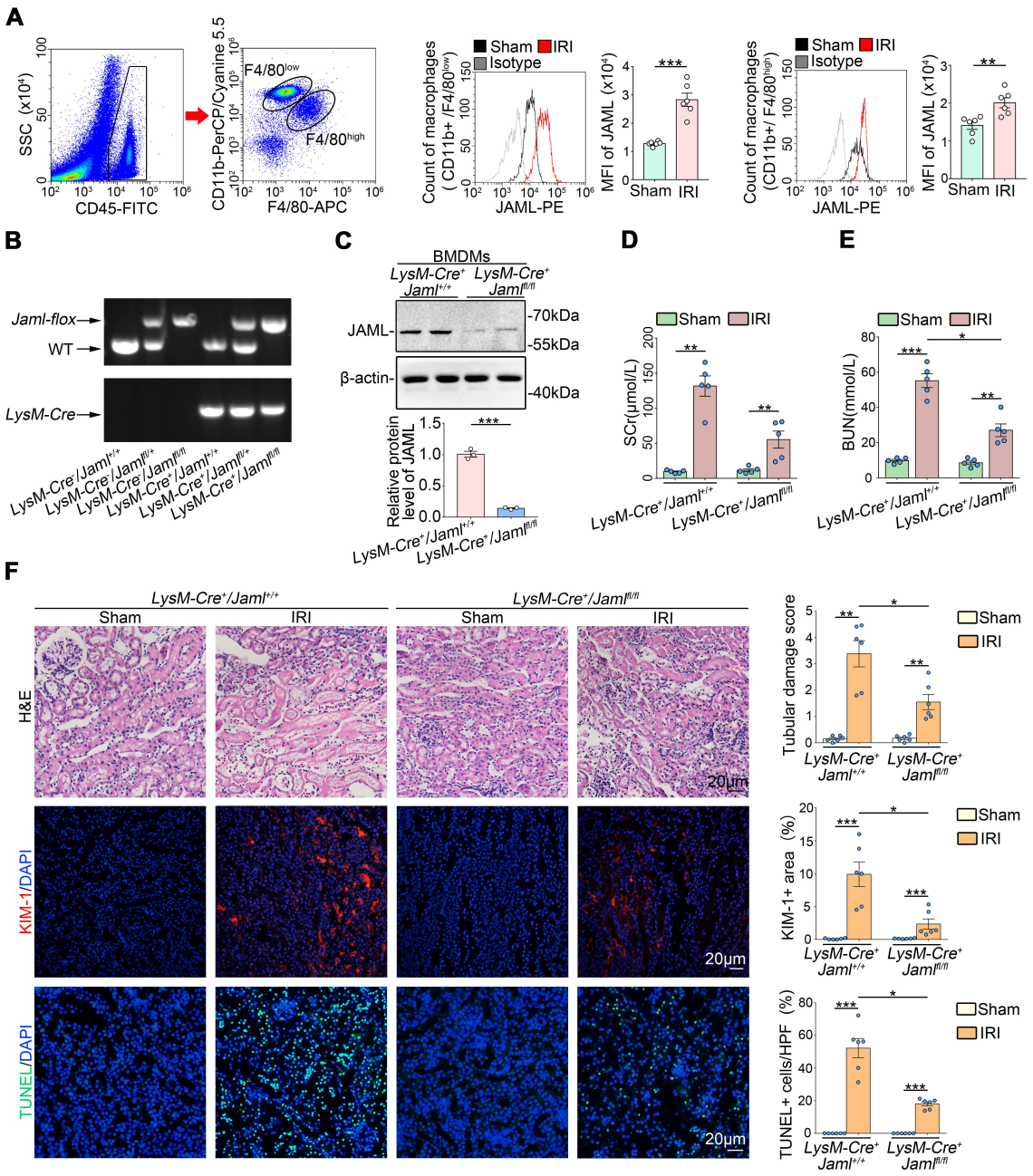

Figure 3. Macrophage JAML was required in the pathogenesis of I/R induced renal injury. (A) Flow cytometry analysis of macrophages freshly isolated from the kidney in mice with renal IRI. CD45-positive cells were divided into the F4/80 ^{low} and F4/80 ^{high} macrophages. Representative histogram showing cell-surface JAML expression on two subsets of macrophages and quantitative analysis of the mean fluorescence intensity (MFI) of JAML-PE. PE, phycoerythrin (n = 6). **(B)** Genotyping was confirmed by tail preparation and PCR at 2 weeks of age (n = 8). **(C)** Representative Western blot and quantifications of JAML expression in the BMDMs from *LysM-cre*$^{+}$/*Jaml*$^{fl/fl}$ mice (n = 3). **(D)** SCr concentration in different groups of mice after renal IRI (n =5). **(E)** BUN levels of different groups of mice after renal IRI (n = 5). **(F)** Representative images of H&E staining and quantitative assessment of tubular damage in the kidney from different groups of mice (upper). Representative images and quantification of IF staining of kidney injury molecule 1 (KIM-1) (red) (middle). *In situ* TUNEL assays and quantification were performed to assess renal cell death (down) (n = 6). Scale bar: 20μm. HPF, high power field. Data are mean ± SEM. **P*<0.05, ***P*<0.01, ****P*<0.001. Two-tailed Student's unpaired t test (A and C), Two-way ANOVA test (D-F).

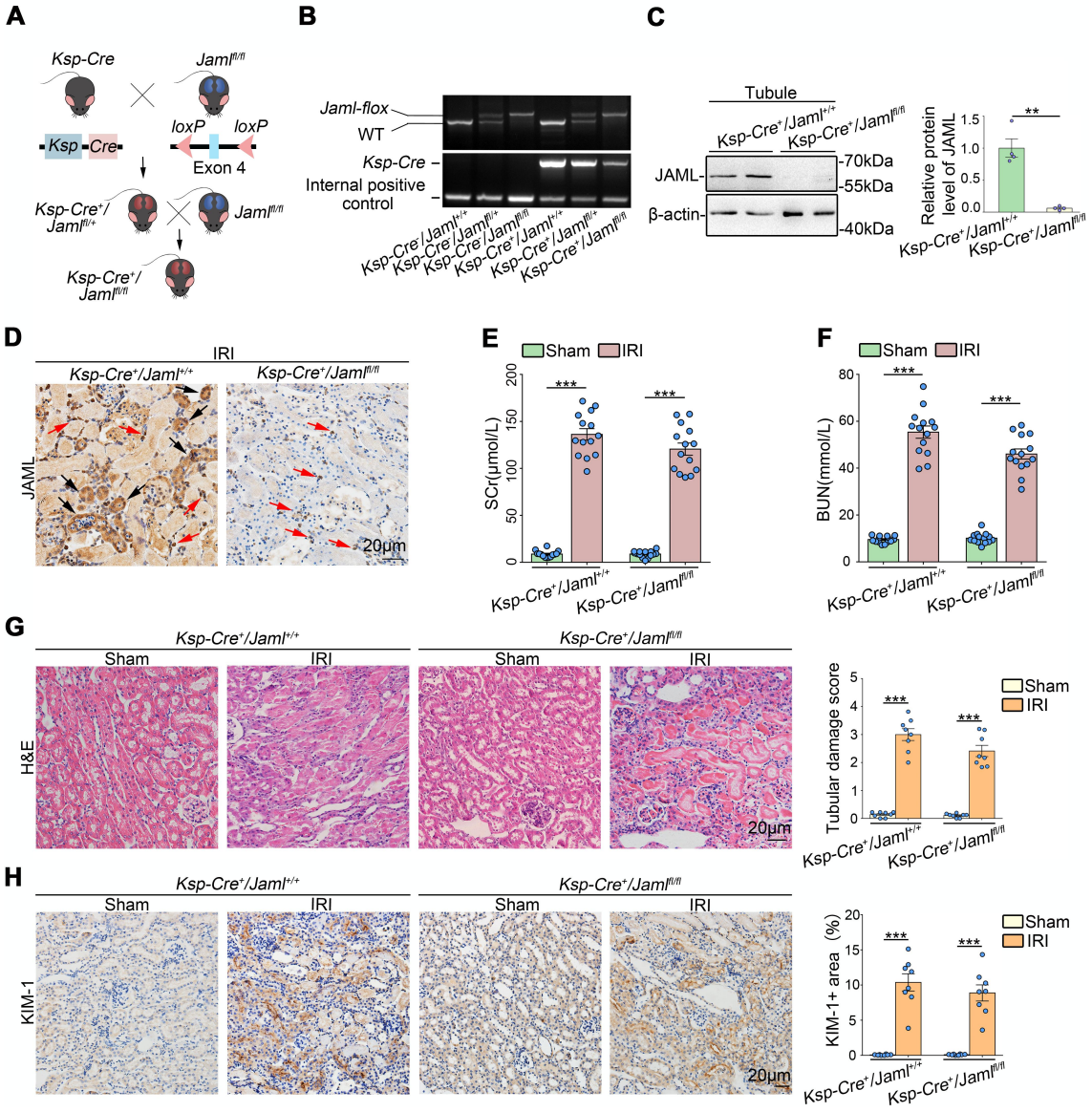

Figure 4. Tubular-specific JAML deletion in mice only slightly ameliorated renal IRI. (A and B) Experimental scheme for generating of conditional knockout mice in which *Jaml* is specifically ablated in renal tubular cells (*Ksp-Cre*$^{+}$/ *Jaml*$^{fl/fl}$) by using *Cre–LoxP* recombination system. Exon 4 is deleted upon *Ksp-Cre* mediated recombination (A). Genotyping was confirmed by tail preparation and PCR at 2 weeks of age (n = 8) (B). **(C)** Representative Western blot and quantification of JAML expression in isolated tubules from *Ksp -Cre*$^{+}$/ *Jaml*$^{+/+}$and *Ksp -Cre*$^{+}$/ *Jaml*$^{fl/fl}$ mice (n = 4). **(D)** Representative IHC images of JAML in the kidney from *Ksp -Cre*$^{+}$/ *Jaml*$^{+/+}$and *Ksp - Cre*$^{+}$/ *Jaml*$^{fl/fl}$ mice with IRI (n = 5). Red arrows indicate representative JAML positive interstitial cells; Black arrows indicate renal parenchymal cells. **(E)** SCr concentration in different groups of mice (n = 14). **(F)** BUN levels of different groups of mice (n = 14). **(G)** Representative images of H&E staining and quantitative assessment of tubular damage in the kidney from different groups of mice (n = 8). Scale bar: 20μm. **(H)** Representative images and quantifications of IHC staining of KIM-1 in the kidney from different groups of mice (n = 8). Data are mean ± SEM. **P*<0.05, ***P*<0.01, ****P*<0.001. Two-way ANOVA test (E-H), Two-tailed Student's unpaired t test analysis (C).

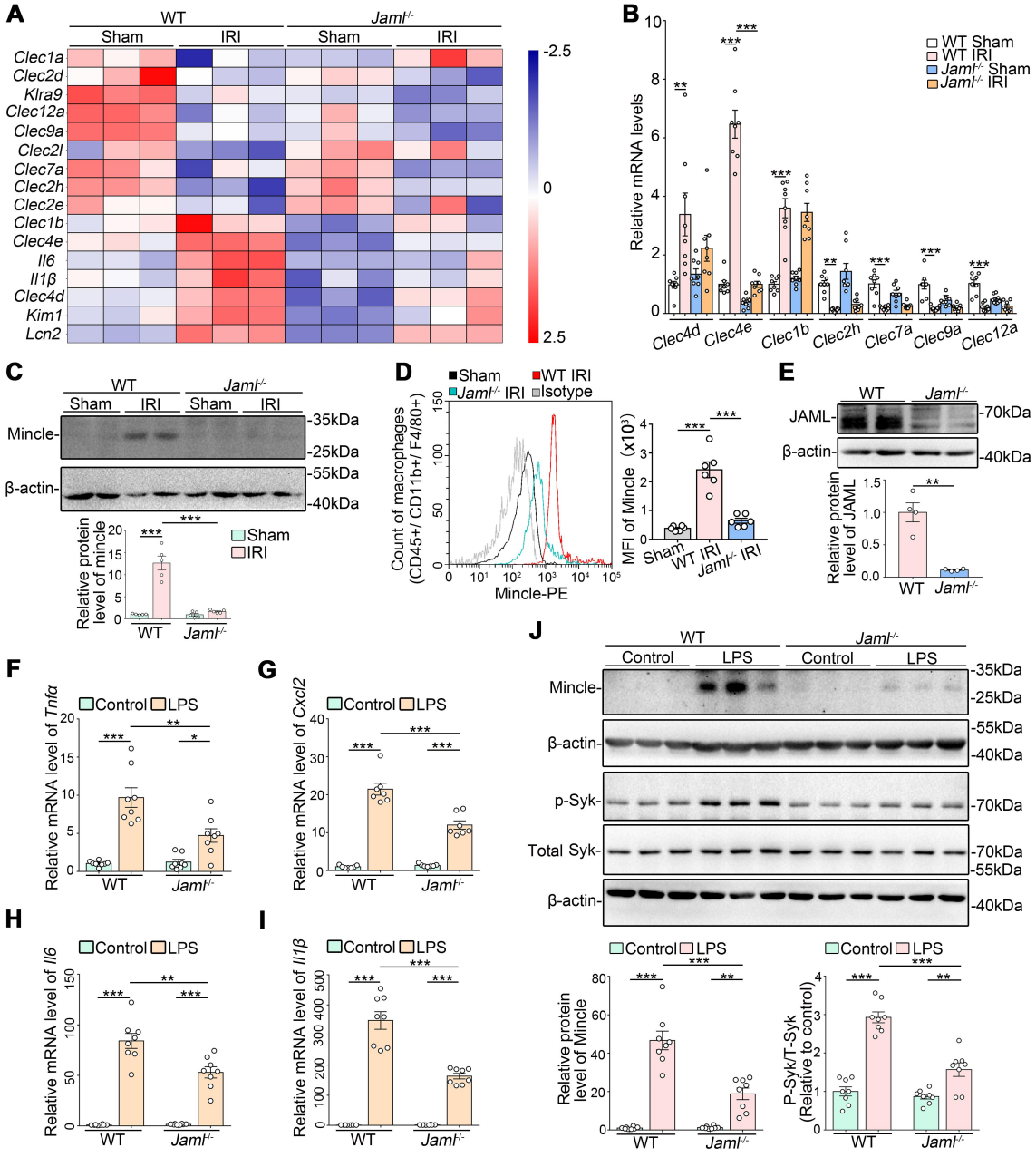

Figure 5. Up-regulation of JAML facilitated C-type lectin receptor Mincle signaling. (A) Representative heatmap of gene expression levels in the kidney from different groups of mice with IRI by microarray analysis (n = 3). Mincle (also called Clec4e). **(B)** Relative mRNA levels of C-type lectin members including *Clec4d, Clec4e (Mincle)*, *Clec1b*, *Clec2h, clec7a, Clec9a* and *Clec12a* in the kidney from different groups of mice (n = 8). **(C)** Representative western blots and quantifications of Mincle in the kidney from different groups of mice (n = 5) **(D)** Representative flow cytometry histogram showing cell-surface Mincle expression on macrophages freshly isolated from the kidney in different groups of mice and quantitative analysis of MFI of Mincle-PE (n = 6). **(E)** Representative Western blot and quantifications of JAML expression in bone marrow-derived macrophages (BMDMs) from WT or *Jaml* $^{-/-}$ mice (n = 4). **(F-I)** Relative mRNA levels of proinflammatory mediators including *Tnfα* (F), *Cxcl*$_2$ (G), *Il6* (H) and *Il1β* (I) in LPS-treated BMDMs (n = 8). **(J)** Representative western blots and quantifications of Mincle, phosphorylated, and total Syk in different groups of BMDMs (n = 8). Data are mean ± SEM. *P<0.05, **P<0.01, ***P<0.001. Two-tailed Student's unpaired t test (E), Two-way ANOVA test analysis (C,D, F-J).

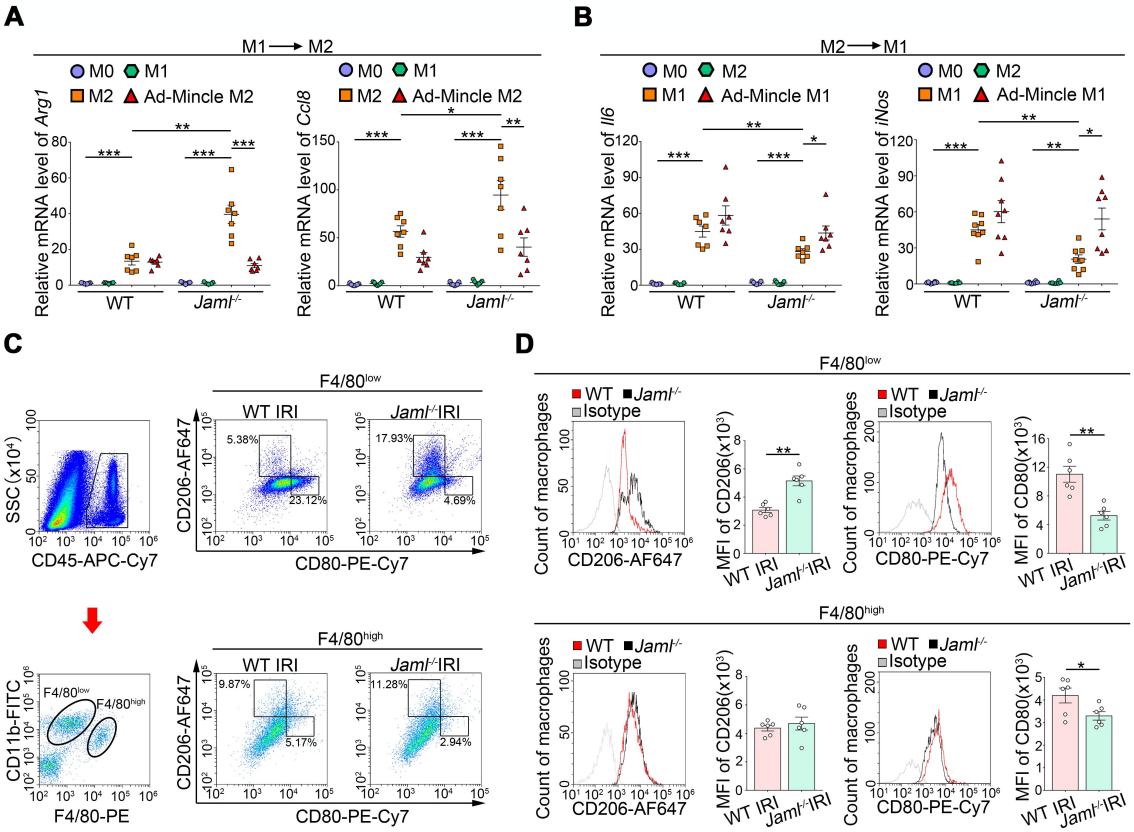

Figure 6. JAML regulated macrophage phenotypic polarization via a Mincle-dependent mechanism. (A and B) BMDM from WT or *Jaml*$^{-/-}$ mice were serum starved for 4 hours (M0) and then polarized to M1 (LPS) or M2 (IL-4) for 8 hours. Media were removed, and then M1 macrophages were treated with M2 stimuli (IL-4), and M2 macrophages were treated with M1 stimuli (LPS) for an additional 8 hours. qPCR was performed to measure *Arg1* and *Ccl8* expression in M1 macrophages polarized to M2 (A). *Il6* and *iNos* gene expression was measured in M2 macrophages polarized to M1 (B) (n = 7). **(C)** Flow cytometry analysis of renal macrophages in the injured kidney after IRI. CD45-positive cells were divided into the F4/80^{low} and F4/80^{high} groups. Representative flow cytometry analysis of M1 (CD80^{high}) and M2 (CD206^{high}) cell populations in F4/80^{low} and F4/80^{high} macrophages isolated from the kidney in different groups of mice. SSC, side scatter. **(D)** Representative flow cytometry histogram showing cell-surface marker CD206 (M2) and CD80 (M1) expression on two subtypes of macrophages and quantitative analysis of MFI of CD206-AF647 or CD80-PE-Cy7 (n = 6). Data are mean ± SEM. *P<0.05, **P<0.01, ***P<0.001. Two-way ANOVA test analysis (A-B), Two-tailed Student's unpaired t test (D).

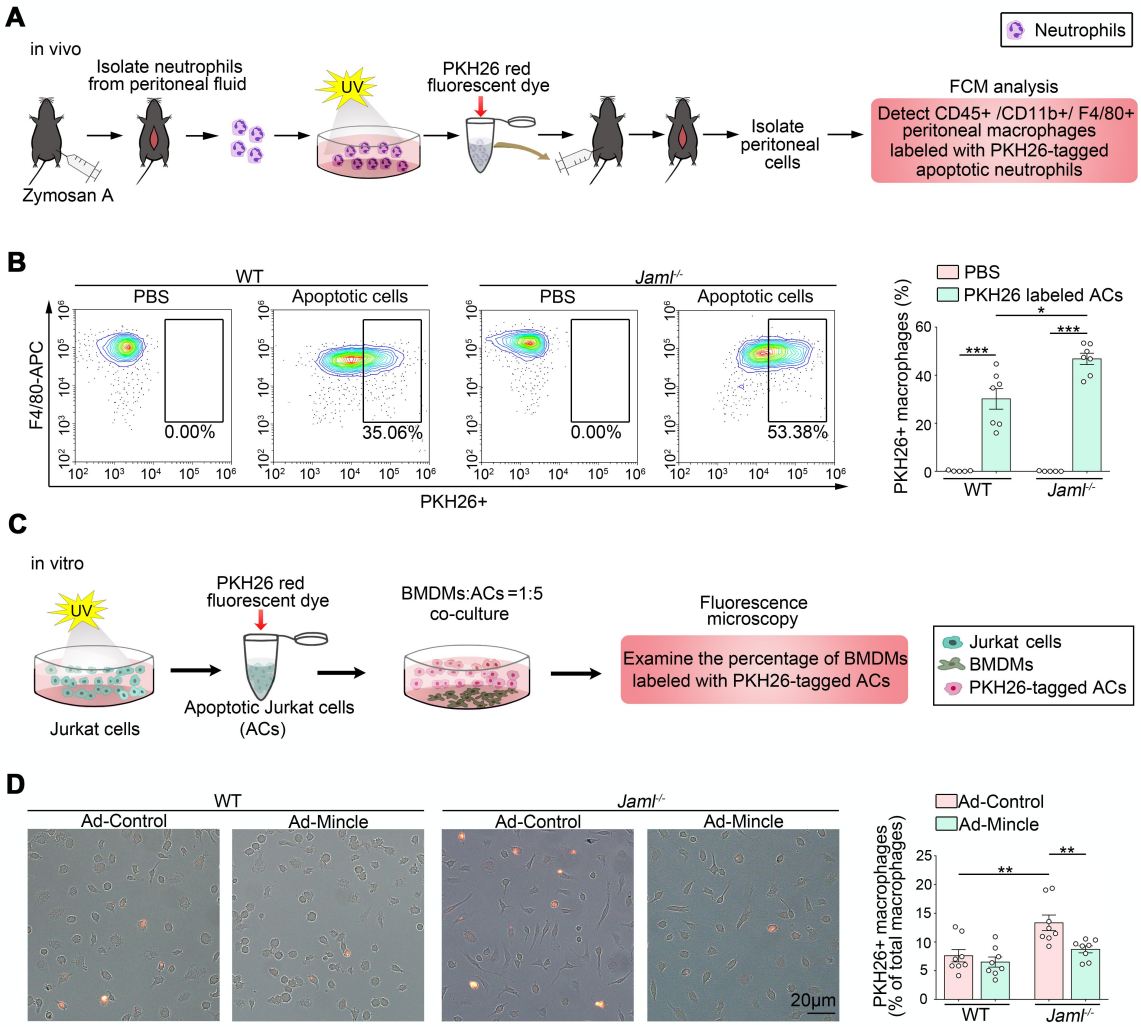

Figure 7. JAML regulated macrophage efferocytosis via a Mincle-dependent mechanism. (A) Schematic diagrams showing the procedure of macrophage efferocytosis assay in vivo. **(B)** Mice was injected by intraperitoneally with PKH26 labeled apoptotic cells (ACs), and 45 min later lavage fluid was analyzed by flow cytometry for the percentage of F4/80+ macrophages that had incorporated the labeled neutrophils (n = 7). **(C)** Schematic diagrams showing the procedure of macrophage efferocytosis assay in vitro. **(D)** Overlay images of phase and fluorescent microscopy images of cultured BMDMs treated for 2h with UV-exposed PKH26-labeled Jurkat cells. Quantitative analysis of percentage of PKH26+ macrophages (n = 8). Data are mean ± SEM. *P<0.05, **P<0.01, ***P<0.001. Two-way ANOVA test analysis (B and D).

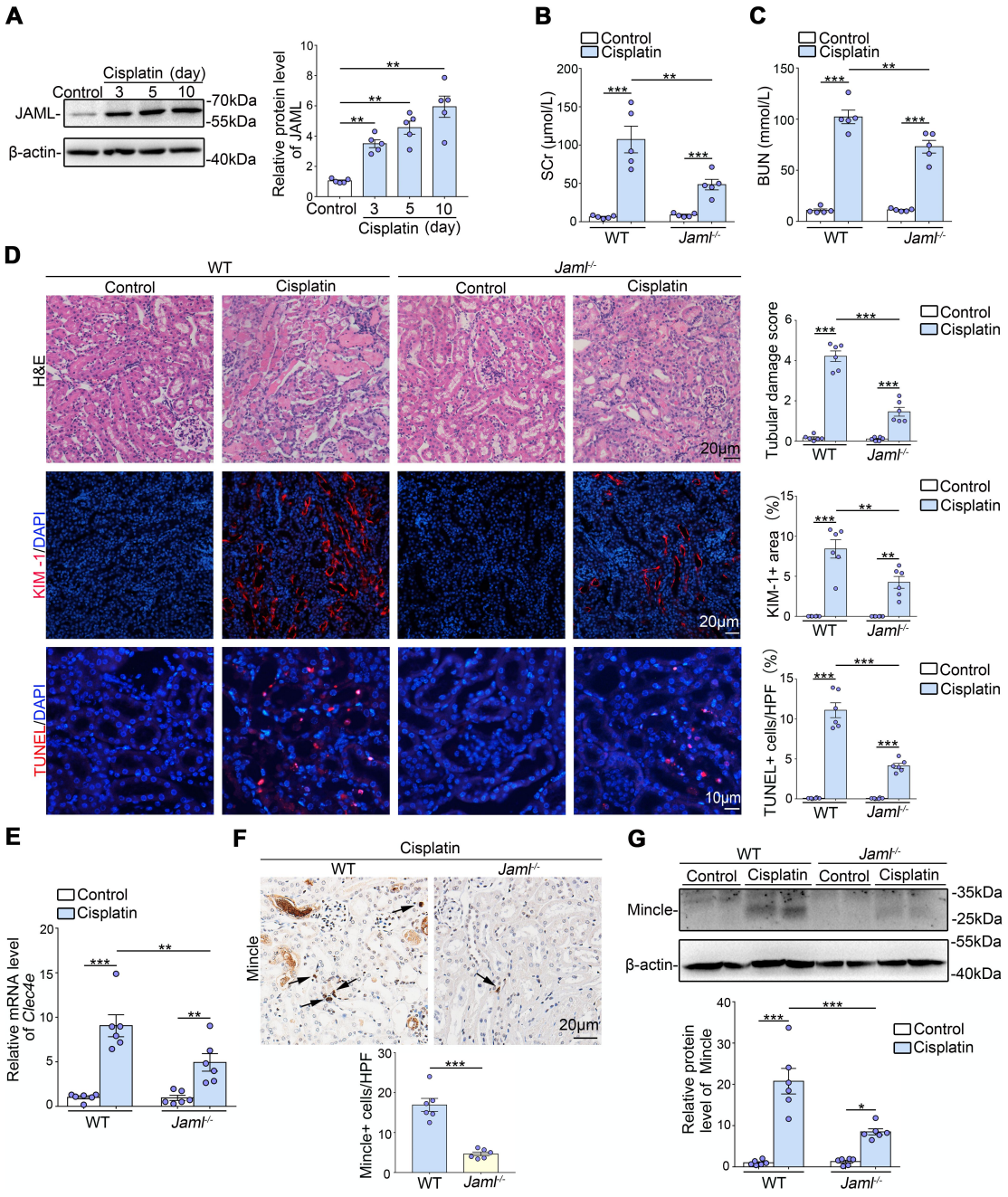

Figure 8. JAML deficiency protected against AKI induced by cisplatin in mice. (A) Representative Western blot and quantifications of JAML expression in the kidney from different groups of mice (n = 5). **(B and C)** Levels of SCr (B) and BUN (C) in different groups of mice (n = 5). **(D)** Representative images of H&E staining showing the morphology of kidney and quantitative assessment of tubular damage (n = 6). Representative images and quantifications of IF staining of KIM-1 (red) in the kidney from different groups of mice (n = 6). *In situ* TUNEL assays and quantification were performed to assess renal cell death (n = 6). **(E)** Relative mRNA levels of *Clec4e* in the kidney from different groups of mice (n = 6). **(F)** Representative IHC images and quantification of Mincle in the kidney from different groups of mice. Arrows indicate macrophages that express Mincle (n = 6). Scale bar: 20μm. **(G)** Representative Western blot and quantifications of Mincle expression in the kidney from different groups of mice (n = 6) Data are mean ± SEM. *P<0.05, **P<0.01, ***P<0.001. One-way ANOVA test (A), Two-way ANOVA test analysis (B-G).

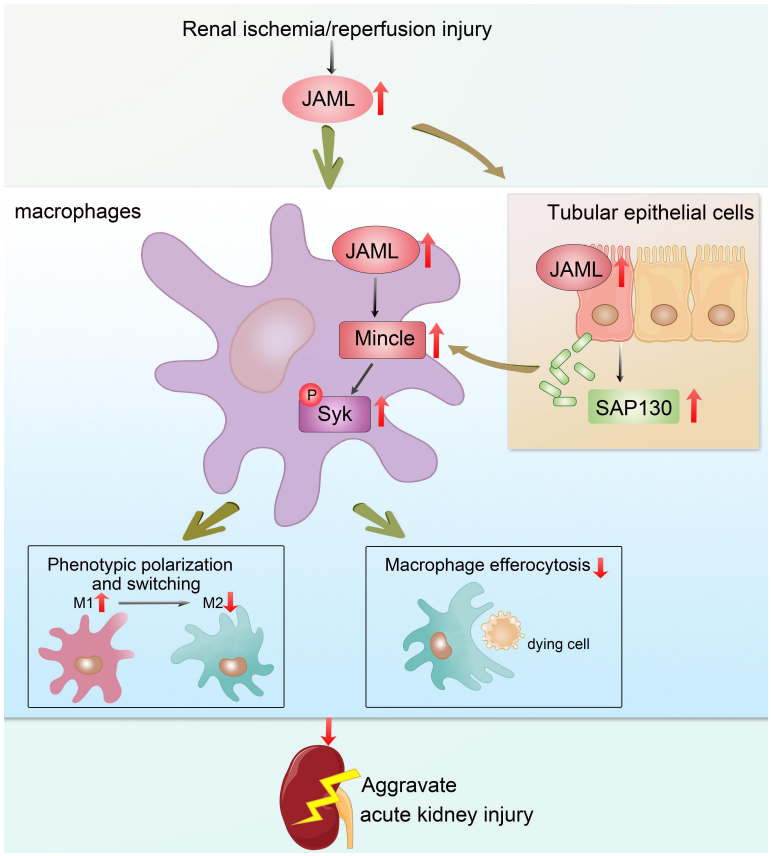

Figure 9. Schematic depicting JAML promotes acute kidney injury mainly through regulating macrophage polarization and efferocytosis via c-type lectin Mincle.